
Article:
Rahimov, E. orcid.org/0000-0001-9557-5808, Baillieu, A., Liu, A. et al. (1 more author) (2024) An investigation of the contact mechanisms between Inconel 718 blades and a NiCrAl-bentonite abradable system. Wear, 556-557. 205465. ISSN 0043-1648

https://doi.org/10.1016/j.wear.2024.205465

An investigation of the contact mechanisms between Inconel 718 blades and a NiCrAl-bentonite abradable system

Eldar Rahimov[1], Aaron Baillieu[1], Allan Liu[1], Matthew Marshall[1]

[1] Department of Mechanical Engineering, The University of Sheffield, Mappin Street, Sheffield S1 3JD, UK

Corresponding author: Eldar Rahimov
E-mail address: eldarrahimov24@gmail.com

Abstract

This work has focused on contact mechanisms between Inconel 718 blades and a NiCrAl-bentonite abradable – a combination commonly used in the hot end of aero-engine compressors, where a transition to high forces and blade wear has been observed in certain contact conditions. In the first set of tests the effects of blade length and rig arrangement were investigated through testing on two different rigs. The purpose was twofold: establishing a connection to the previous research performed on the slower of the two rigs, and developing a general understanding of the effects of these two parameters on results. It was demonstrated that both rig stiffness and blade length in the considered range did not have a strong effect on the likelihood of transition of a test to the aforementioned high wear regime. The higher speed rig was then used to investigate the progression to high contact forces and blade wear in more detail by performing tests at speeds of 200m/s and 280m/s, with three incursion rates considered at each speed. Test to test variability was similarly investigated by performing five repeats for each test condition. Two distinct contact modes were observed – one where forces remained low and no blade wear occurred, and another where forces progressively increased until blade wear initiated and forces stabilised at significantly higher values than in the case of low force tests. These contact modes were explained through interaction between the incursion rate and rate of abradable fracture. The results have shown that an increase in incursion rate has increased the likelihood of the high-force contact mode, and an increase in blade tip speed decreased it. The inherent randomness of the abradable spraying process was demonstrated to lead to variability in material properties for nominally similar samples, and in turn the transition in contact mode was in essence probabilistic in nature. This variability also highlighted the importance of performing repeats when contacts with sprayed abradable materials are considered.

1 INTRODUCTION

Abradable materials are commonly utilised as sacrificial coatings in components such as aero-engine compressor and turbine casings. These materials are designed to abrade when in contact with rotating blades creating a sealing surface and reducing aerodynamic losses. When a contact occurs wear mechanisms which promote effective removal of abradable surface and allow to minimise blade wear are desired to ensure effective sealing. Some modelling [1, 2, 3] and, largely, experimental methods are commonly utilised to improve the understanding of wear mechanisms in contacts with abradables.

Some of the experimental work performed on abradable materials included characterisation of mechanical properties such as hardness testing as abradables are sprayed to a designated hardness range [4], sliding wear volume [5] and scratch testing [6, 7]. However, mechanical properties alone showed only a limited ability to predict the outcomes of abradable-blade contacts due a number of different wear mechanisms occurring depending on multiple contact parameters.

Most of the research on understanding abradable-blade mechanisms was performed using experimental test rigs. Primary focus of experimental research was on AlSi-based abradable materials with Borel et al. producing a first set of wear maps for this material type [8]. These tests were performed on a highly representative rig, which was later also used by Bounazef et al. [9]. The wear mechanisms in contact with this type of materials were later investigated in further detail by multiple authors using the scaled rig at the University of Sheffield [10, 11, 12], and rigs at the Zhejiang University [13] and Chinese Academy of Sciences [14, 15].

While a lot of focus was given to the AlSi-based abradables used in lower temperature stages of compressor, at present, only limited research has been conducted on the contact between Inconel 718 blades and NiCrAl-bentonite abradables, despite this being a blade-liner contact that occurs at a number of stages in the hot end of the compressor. The majority of results to date originate from studies conducted by Taylor et al. [16] and Watson et al. [17, 18], where both authors highlighted the influence of both the rates of blade incursion into the liner and blade tip speed on test outcomes.

Both authors note that at low rates of blade incursion into the liner, removal of abradable material occurs without blade wear, whereas at very high incursion rates, significant abradable compaction takes place accompanied by blade wear. As part of the work by Watson, a wear model was proposed, whereby at low incursion rates abradable material was removed by the blade via a sub-surface damage accumulation and fracture mechanism, with the rate of material release failing to keep up as the incursion rate is increased, leading to increased blade wear. However, it was unclear at what incursion rate does blade wear initiate and how gradual is increase in contact forces and blade wear with an increase in incursion rate. The better understanding of transition to blade wear is of practical interest given that many in-service rubs are expected to occur at incursion rates within this region.

Whilst the work by Watson suggested that blade speed had some contribution to the wear of NiCrAl-bentonite abradables, the work of Taylor indicated that a significant reduction in blade wear occurred with an increase in blade speed at the lowest incursion conditions. However, in both cases, blade speeds were below the typical values of 300-400m/s experienced by aero-engines in service, and limited to 200m/s and 152m/s respectively.

As such, whilst the model proposed by Watson offers a convincing explanation for the wear behaviour observed, and Taylor evidence that blade speed is also an important variable, a clear need exists to explore the transition to blade wear in more detail, as well as extend the work to more engine representative blade tip speeds. This work attempts to address this by exploring the region at which the transition to blade wear is expected in more detail through tests at multiple incursion rates around this region using a high speed test platform capable of achieving blade speeds of 280m/s. This rig has been previously used to investigate the wear mechanism of AlSi-polyester based abradable materials when incurred with a titanium blade [19], and is instrumented to measure contact force and blade wear during a rub test, meaning that it is well placed to investigate when the wear mechanism transitions.

Given that the variation in properties of abradable materials is often significant as a consequence of the thermal spraying processes through which they are manufactured, an unanswered question also remains as to how binary this transition to blade wear is for a given batch of material, where results for similar wear mechanism transitions for AlSi-polyester and AlSi-hexagonal boron nitride based abradables might suggest a more probabilistic aspect to this change [19, 20, 11]. This will be addressed in this work by performing a number of repeats at each of the considered incursion rates.

However, it is also of note that the updated high-speed test platform has been developed with a reduced blade length when compared to that utilised by Watson in his study, and also that the shaft onto which the disc is mounted is supported on either side by built-in bearings, where the previously used test apparatus had a cantilever arrangement. These changes in test arrangement are of particular note given that both studies highlighted abradable compression as a key part of the wear mechanism observed, with Watson going further in hypothesising that abradable material removal is via a sub-surface damage accumulation and fracture mechanism. Whilst unlikely that the blade and test rig stiffness play a significant role in this mechanism given the instantaneous nature of the blade strike, this cannot be ruled out. As such additional tests will be performed on the lower speed test rig previously used by Watson with both long and short blades, at identical conditions to those tested on the high speed rig, so as to determine what role, if any, blade and rig stiffness contribute to the wear mechanisms detailed.

2 MATERIALS AND METHODOLOGY

The abradable samples used in this study are NiCrAl-bentonite manufactured from a powder of bentonite particles chemically clad with NiCrAl, deposited using a thermal spraying

process. This material is available commercially as Metco 314 ns (Oerlikon Metco, Switzerland). The manufactured abradable samples are tested against Inconel 718 blades of two different lengths, with this combination of abradable and blade material matching that typically found in the high pressure stages of the compressor in commercial aero-engines. Figure 1 shows images of the abradable sample alongside the standard blade design used in this work.

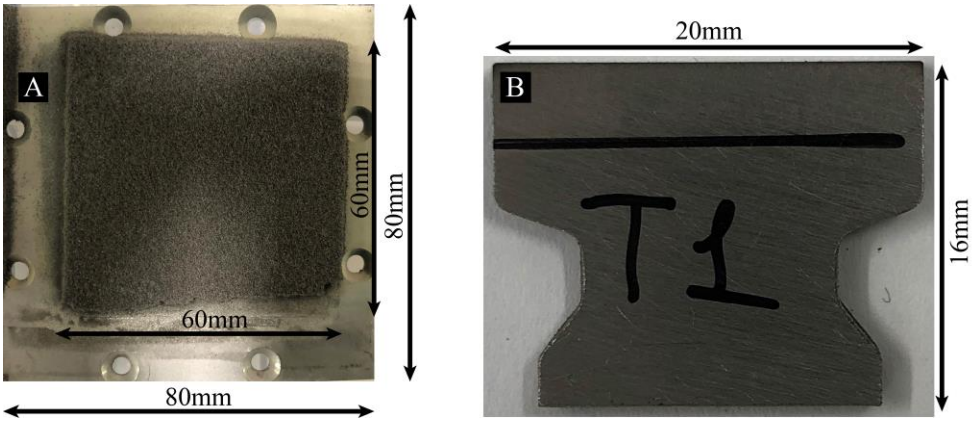

Figure 1 – a) The standard NiCrAl-bentonite abradable sample, b) the standard blade with 4mm stick-out from a blade holder, the blade thickness is 2mm. The blades with 7mm stick-out are identical in design except for blade length being 19mm rather than 16mm.

Tests in this work were performed on two scaled test rigs at the University of Sheffield, both of which have been previously described in detail [19, 20]. The first of these two rigs, herein referred to as the Low Speed Rig (LSR), consists of a grinding spindle that drives a disc with a test and dummy blade mounted within it, with the dummy blade included to balance the system. The spindle is capable of achieving blade tip speeds of 200m/s, with the rotating blade then incurred into an abradable sample mounted on a z-axis microscope stage directly below it. Figure 2 shows the test set up, where an in-situ measurement system captures blade wear, force and temperature data throughout a test. Blade wear is measured using a stroboscopic imaging system as detailed in [20], where the blade side is exposed on a pass-by-pass basis using an LED synchronised to the rotation of the disc via a light gate and strobe controller (Gardasoft RT200F-20, Stemmer Imaging Ltd., Surrey, UK), and images recorded using a machine vision camera. Similarly, contact force is measured via a 3-axis piezoelectric force transducer (Kistler Instruments Ltd, Hook, (UK), Type 9347C), installed between the abradable sample and microscope stage. Finally, temperatures are monitored during the rub event using a non-contact infrared pyrometer (Micro-epsilon, Koenigbacher, Germany), targeted at the centre of the rub track. The second rig used in this study, herein referred to as the High Speed Rig (HSR), is similar in concept to the LSR, aside from the fact it is able to reach higher blade tip speeds (280m/s). The disc is mounted on an axle supported by built-in bearings, and the microscope stage is now replaced with a linear actuator. The HSR is shown in Figure 3, where it should be noted that the same

instrumentation as previously detailed for the LSR is installed on the test rig. Further details on the rig can be found in [19, 18].

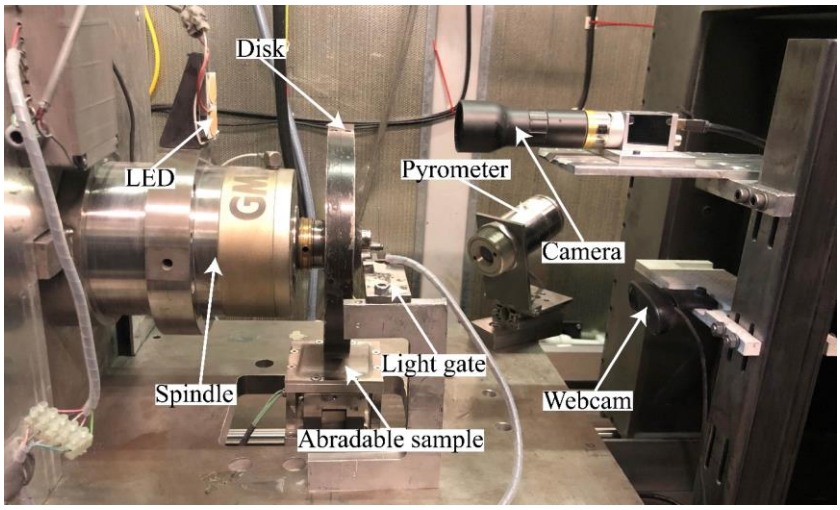

Figure 2 – The low-speed rig image, side view.

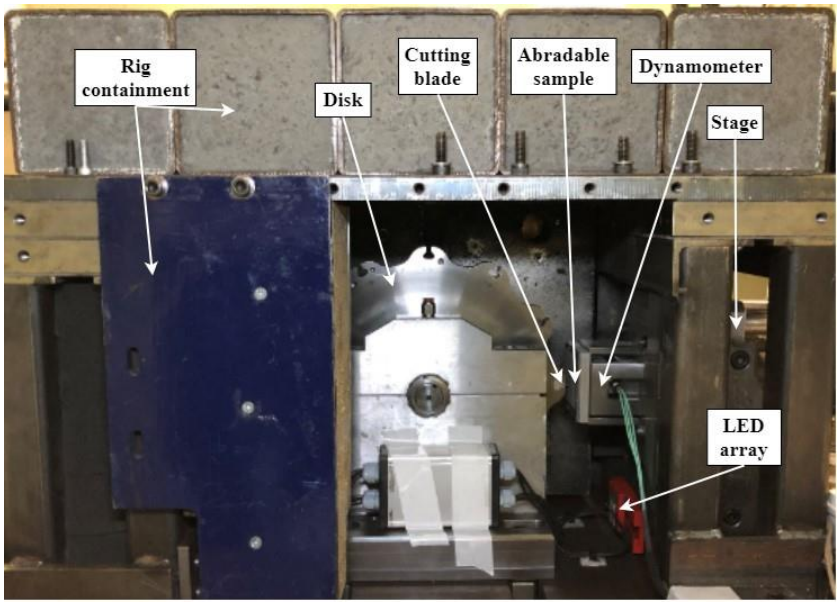

Figure 3 – The high-speed rig image, front view. Figure reproduced from [19] with kind permission of the authors and Elsevier.

The tests on both rigs are performed at room temperature, which is significantly lower than the operational temperatures seen in the hot end of aero-engine compressor. However, it was previously shown that flash temperatures in contacts between blades and abradables can reach representative values within seconds based on the results by Wang [21] and Emery et al. [22]. High temperatures are reached quickly due to a combination of the high forces / poor thermal diffusivity of the abradable, meaning that even for the shorter 10 second tests, largely representative temperatures would have been reached. Additionally, no differences are expected between tests at room and elevated temperatures due to sintering of abradables at elevated temperatures due to two reasons: very short duration of tests in the order of

seconds to minutes, and as abradable samples are pre heat treated until a stable hardness value is reached as discussed further in section 2.1.

In order to perform a test on both rigs, the abradable sample is first moved so that it just touches the blade sample, with this contact point determined to an accuracy of 10µm via a binary search procedure. Next the abradable sample is retracted by 500µm and the spindle rotated to the desired test speed. Finally, the abradable sample is driven into the rotating blade at a programmed incursion rate, and once the planned incursion depth is reached, the abradable sample is retracted.

As highlighted, given the previous study by Watson et al. [17] utilised the LSR and blades of longer length than can be used on the HSR, and blade and test rig stiffness have a potential impact on the material removal mechanism, tests were first performed to investigate if this is indeed the case. Table 1 shows a series of tests performed between the LSR and HSR with varying blade lengths. In the case of the 7mm blades, this measurement represents how far the blade projects out unsupported from the disc, and is the same as for those used previously by Watson et al. [17]. Whereas, in the case of the 4mm blades, these represent the new design used on the HSR rig. As shown in the Table, the effect of the blade length change is first explored, before the impact of the difference in disc arrangement between the two rigs. In each case, tests were conducted at 200m/s on both rigs, as this represented the maximum speed of the LSR, and at an incursion rate of 0.06µm/pass. This incursion rate was chosen based on modelling work undertaken in the previous study [17], and identified as an incursion rate where whilst forces were likely to be significant and any influence on behaviour due to blade or rig stiffness apparent, wear was unlikely to yet occur.

Table 1 – The test matrix for the first experimental part.

Test	Rig	Blade / mm	Speed / m/s	Incursion rate / µm/pass	Rub depth / µm	Repeats
1	LSR	4	200	0.06	1000	3
2	LSR	7	200	0.06	1000	3
3	HSR	4	200	0.06	1000	3

Following on from investigating the initial tests outlined, a further series of experiments were performed to explore the incursion conditions at which a transition to blade wear initiated. The test conditions chosen are shown in Table 2, and were once again chosen based on the work of Watson et al. [17], although in this case focused on incursion conditions where forces were expected to increase significantly. As shown in the Table, testing was performed at two different blade tip speeds (200m/s and 280m/s), and three incursion rates that were selected based on the blade tip speed. The incursion rates used for the tests at 200m/s were 0.06µm/pass, 0.10µm/pass and 0.14µm/pass. In the case of tests at 280m/s, the incursion rates selected were higher due to expected improved wear behaviour at the higher

speed. Such an improvement was previously demonstrated by both Taylor et al. [16] and Watson et al. [17], with incursion rates of 0.14µm/pass, 0.22µm/pass and 0.30µm/pass chosen in this case. To establish the probability of transition occurring for a given test condition, five repeats were done in each case, resulting in a total of thirty tests for this stage of the study.

Table 2 - The test matrix for the second experimental part.

Test	Rig	Blade / mm	Speed / m/s	Incursion rate / µm/pass	Rub depth / µm	Repeats
1	HSR	4	200	0.06	1000	5
2	HSR	4	200	0.1	1000	5
3	HSR	4	200	0.14	1000	5
4	HSR	4	280	0.14	1000	5
5	HSR	4	280	0.22	1000	5
6	HSR	4	280	0.3	1000	5

2.1 Hardness Testing

All the tests in this study were done with samples from a batch with a nominal hardness of H50 (measured on the HR15Y Superficial Rockwell Hardness Scale), heat treated at 750°C for 100 hours, as previous studies had highlighted that blade wear was more likely with this material hardness. The heat treatment of samples results in an increase in sample hardness. The heat treatment is reflective of ageing typically occurring in service, with 100 hours chosen as previous results have demonstrated that by this time a stable hardness value is reached. The blades are made from Inconel 718 and have a nominal room temperature hardness of around 36-45 on the HRC Rockwell Hardness Scale based on the material data sheet [23].

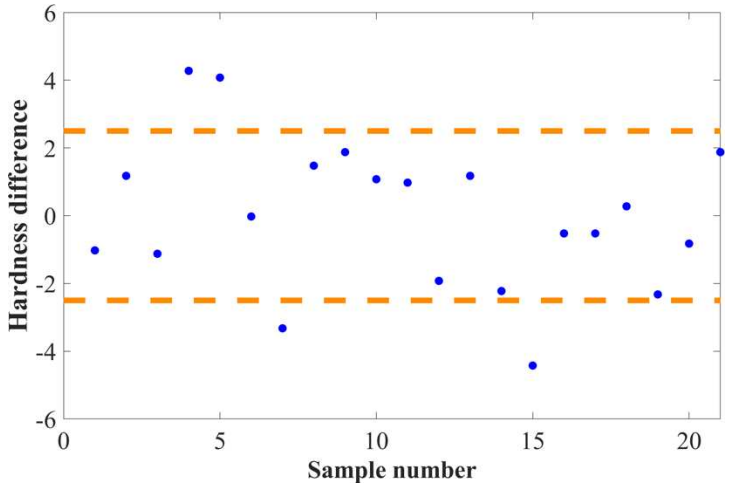

Figure 4 - The measured hardness deviation for the 21 NiCrAl-bentonite samples of the same nominal hardness from the average measured hardness for the batch.

In order to further investigate the repeatability of the thermal spraying process, twenty-one additional samples were manufactured, heat treated and hardness tested in nine separate locations, to establish the statistical variation in hardness present. The difference between the measured average hardness values for all 21 samples and the average value for the batch is given in Figure 4, where the dashed lines show the 2.5 points deviation from the mean value, which was considered a level of deviation with the potential to influence the wear mechanism based on previous research with sprayed NiCrAl-bentonite coatings [18].

As shown in the Figure, the average hardness for the majority of samples was very close to the average value for the batch. For 17 out of 21 samples (81%), the average hardness value was within the defined threshold. However, some of the samples were outside of the threshold, with 2 being hard and 2 soft. This showed that there is a possibility of outliers occurring in the performed tests due to variations in hardness of samples within a batch, and in turn highlights the importance of performing repeats to confirm that observed trends are repeatable and are not due to the presence of outliers. However, at the same time, it should be noted that the observed variation in hardness is reasonable for NiCrAl-bentonite samples manufactured via thermal spraying.

3 RESULTS

In this section, results obtained with 4mm and 7mm blades on the low-speed rig, and with 4mm blades on the high-speed rig are first presented. After, results from the tests completed on the high-speed rig focused on improvements in the understanding of transition to high contact forces and blade wear are shown. The primary focus is given to the force data obtained with a dynamometer as it was previously shown that forces are a good indicator of contact conditions in tests with the NiCrAl-bentonite abradable [17]. Post-test images of blades and abradable samples and blade wear results in the form of blade profile history maps (more details on blade profile history maps construction can be found in [19]), are also presented to further support the observations as appropriate.

3.1 Tests with the blades of different lengths on the LSR and HSR

The force data plotted against rub length (4) for all the nine tests completed for the first experimental stage are presented in Figure 5, where it should be noted that rub length represents the total sliding distance of the blade over the incursion event.

As shown in Figure 5, a similar pattern was observed in the results for all of the three investigated test conditions. Out of the three tests at each of the test conditions, two had low contact forces and one of them transitioned to high contact forces.

This result suggests that differences in rig stiffness and between 4mm and 7mm blades do not lead to significant differences in test outcomes, and is insignificant when compared with variables such as incursion rate, abradable hardness and blade tip speed identified by multiple previous authors [16, 17].

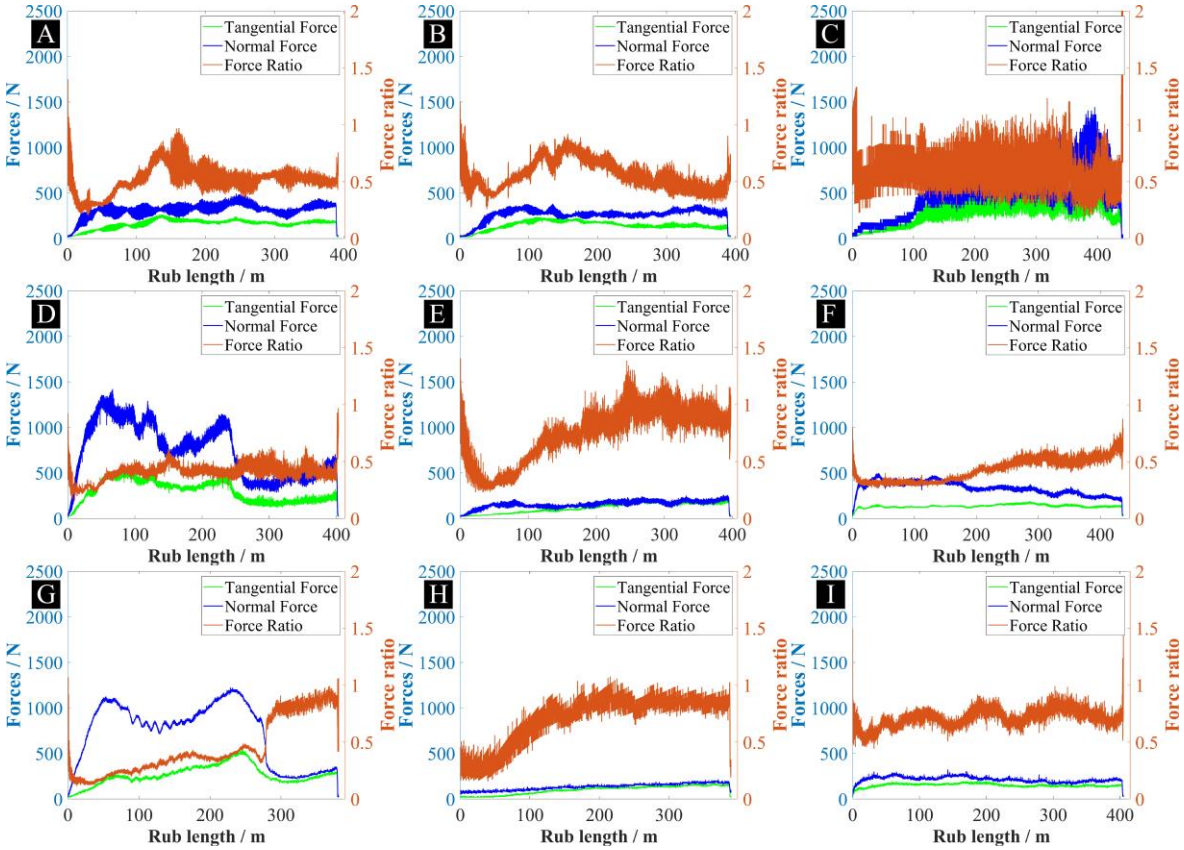

Figure 5 - The force data for the tests completed at 0.06µm/pass, 200m/s on the low speed rig with a,b,c) 4mm blades, d,e,f) 7mm blades, and g,h,i) high-speed rig with 4mm blades

Interestingly, in this set of results it can be clearly seen that very different contact forces can occur for identical test conditions. For the tests where a sharp increase in forces was not seen, the maximum normal force was limited to 300-500N, while for tests where such an increase occurred, the maximum normal force was as high as 1200-1500N, indicating at least a threefold increase in the maximum normal force. In the next two sections, the transition between the two contact modes (with low and high contact forces) will be investigated in more detail, where such changes in contact force will be further explored.

3.2 Transition incursion rate at 200m/s

At this blade speed, three incursion rate conditions (0.06µm/pass, 0.10µm/pass and 0.14µm/pass) are investigated with five repeats for each condition, totalling fifteen tests. Clear differences in the number of tests that transitioned to the high forces can be seen based on the considered incursion rate. In order to illustrate this point, first, a comparison of two tests where a transition was and was not observed is shown, highlighting the differences in how the test progressed and test outcomes. This is followed by a histogram summarising the test results for all the 15 tests at 200m/s. Each test on the histogram is plotted individually to show the total number of tests that transitioned to high contact forces for each incursion condition and to further highlight the significant differences between the two occurring

modes of contact: the contact forces are either relatively low with no blade wear or high with some blade wear.

To illustrate the differences in wear behaviour between tests that did not transition and that transitioned, a blade profile history map, accompanied by post-test images of the abradable and blade and force data throughout a test are given for repeats 1 and 2 at the 0.10 µm/pass incursion rate in Figure 6 and Figure 7 respectively.

As shown in Figure 6b. whilst forces for the test that did not undergo transition increased throughout the test, this increase was small, and the normal force stabilised at around 250N. Whereas, as shown in Figure 7b, for the transitioned test the increase in forces was rapid, with the normal force stabilising around 1200N, and some cyclic behaviour in force seen once blade wear initiated. Such a difference in the maximum normal force is consistent with what was observed in the previous section where transition to a high force contact situation occurred.

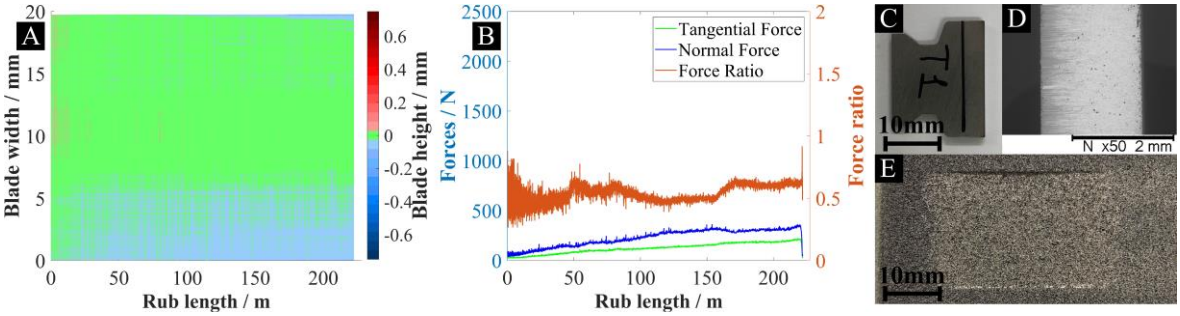

Figure 6 - Results for the repeat 1 at 0.10µm/pass, 200m/s with H50 abradable a) the blade profile history map, b) forces during the test, c) post-test image of the blade, d) post-test SEM of the blade, e) post-test image of the abradable sample. This test did not transition to the high-force contact mode.

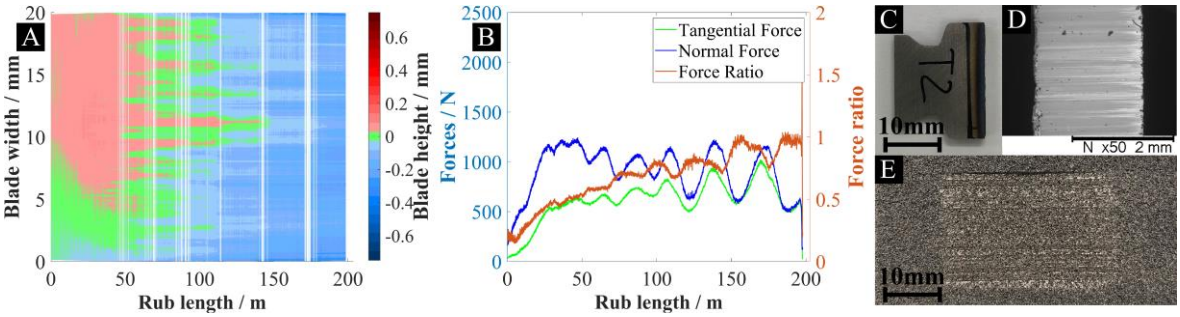

Figure 7 - Results for the repeat 2 at 0.10µm/pass, 200m/s with H50 abradable a) the blade profile history map, b) forces during the test, c) post-test image of the blade, d) post-test SEM of the blade, e) post-test image of the abradable sample. This test transitioned to the high-force contact mode.

Moving on to wear, clear differences can be seen on the wear history maps and from post-test images of the samples. As shown in Figure 6c, for the test that did not transition, the

blade appears undamaged, only mild discolouration at the blade trailing edge can be seen in Figure 6d, and, as shown in Figure 6a, virtually no wear can be seen on the blade profile history map. On the other hand, for the test, that transitioned, it can be seen on the blade profile history map that blade wear initiated and propagated across the blade front (Figure 7a). Thermal damage can also be seen on the blade in Figure 7c, and thermal discolouration is seen across the entire blade thickness in Figure 7d.

To further support these observation, SEM and EDS analysis were performed on the blades from these two tests as shown in Figure 8. It can be seen that for the blade from repeat 1, which did not transition, aluminium and oxygen are more pronounced only towards the edge of the image, while for the blade from repeat 2, strong presence of aluminium, silicone and oxygen is seen across most of the thickness. The strong presence of aluminium and silicone might suggest some transfer from the abradable surface as oxides of these two elements are parts of bentonite. Small amounts of aluminium and silicone (<1%) are also present in the base Inconel 718 alloy, so another cause of such surface appearance could be oxidation of these elements on the surface layer due to very high contact temperatures.

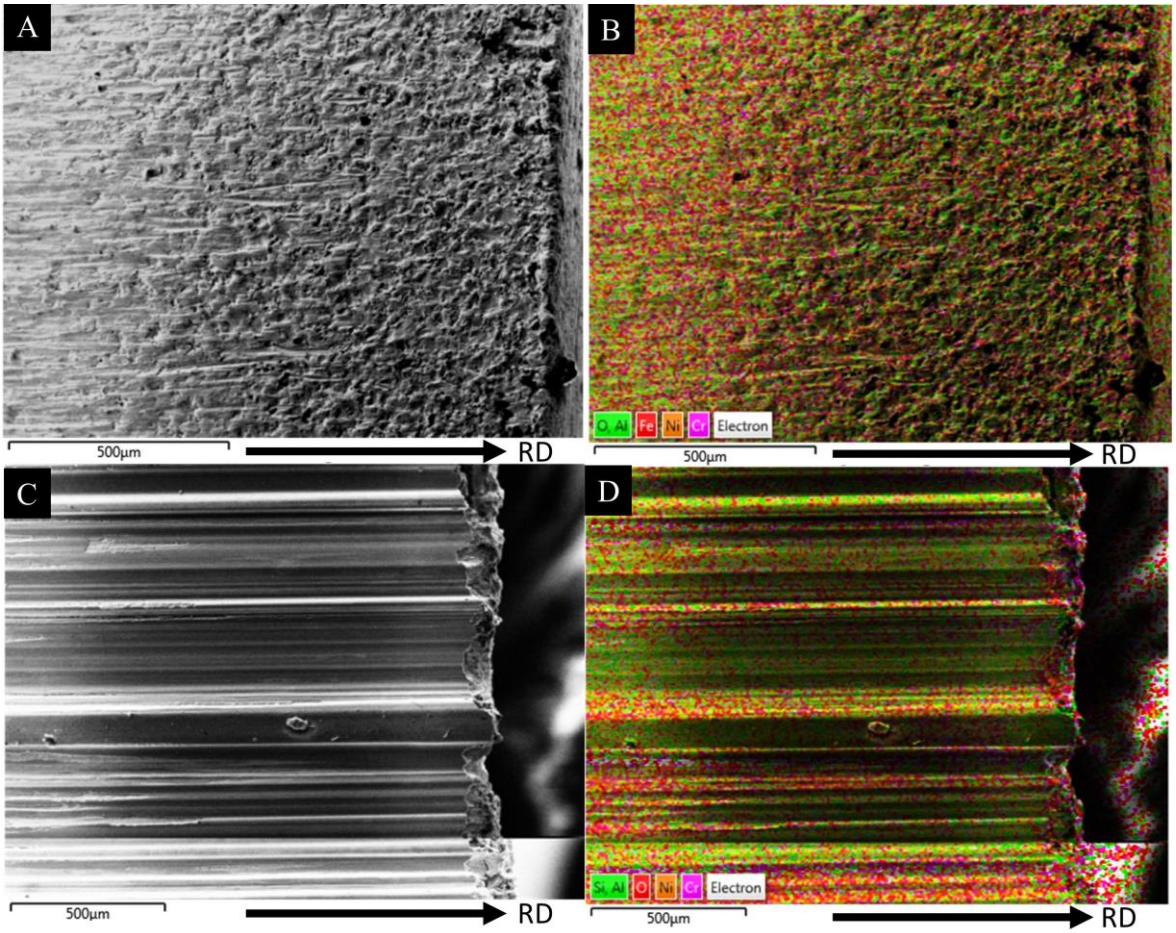

Figure 8 - a) SEM image for the blade from repeat 1, b) EDS layered image for the blade from repeat 1, c) SEM image for the blade from repeat 2, d) EDS layered image for the blade from repeat 2. Rub direction is indicated with an arrow and RD note under each image.

Comparing Figures 6e and 7e, abradable surfaces for both tests look broadly similar, and are rough with the microstructure resembling the as-sprayed condition. This is for example, very different to the tests with AlSi-polyester abradables, where surfaces were shaped by the blade tip and very little roughness was seen along the rub track [19]. Whilst the surfaces for the two tests are similar, it is noticeable that in the case of the transitioned test (Figure 7e) the surface has localised spots that appear shinier than the rest of the surface, which could be due to transfer of Inconel 718 from the blade due to wear.

To check whether transfer has occurred, SEM and EDS layered images of rubbed abradable surfaces from both tests were taken in several locations on the abradable as shown in Figure 9. Both surfaces look similar with strong presence of nickel phase and globular silicone and aluminium particles. On the abradable surface from the second repeat more flat regions are present which are likely the result of the rub with chromium layer seen on some of them. It can be seen in Figure 10 that chromium rich region in the first imaged location from the second repeat coincides with an iron rich region. The presence of chromium and iron layers suggests that some blade transfer has indeed occurred, as both are constituents of the Inconel 718 alloy. However, it is difficult to identify if chromium and iron rich zones are correlated with shiny spots in Figure 7e. The potential of blade transfer is also supported by previous research where it was shown that such transfer occurs for test conditions, where blade wear was observed [17].

The force and blade length results for all the 15 tests at 200m/s are summarised in Figure 11, where it is apparent where tests transitioned to the high force wear mechanism at a given incursion rate. Mean blade wear was obtained by averaging the blade length change at all blade width locations at the end of a test, and gives a useful indication of the overall relationship between contact force and wear in this context.

As shown in the Figure, it can be seen that at the 0.06µm/pass incursion rate, one test had high forces, while at 0.10µm/pass and 0.14µm/pass, three and five tests had high forces respectively. These results showed that at the speed of 200m/s, the transition between the two contact modes occurs over a range of incursion rates for the samples in a given batch.

The trend in blade wear results followed the trend in contact forces. For all of the tests that transitioned, apart from repeat 2 at 0.06µm/pass and repeat 5 at 0.10µm/pass, significant blade wear was observed. No significant blade wear was seen for these two tests because despite a temporary period of high forces, forces decreased latterly in the test indicating that abradable fracture improved. This variation in behaviour is shown in both Figure 12a and Figure 12b for these tests, where high forces are only temporary. Such behaviour is in contrast to repeat 5 at 0.14µm/pass (Figure 12c), where the maximum achieved force was similar, but no decrease in forces occurred, with forces maintained at or around the maximum value leading to more significant blade wear.

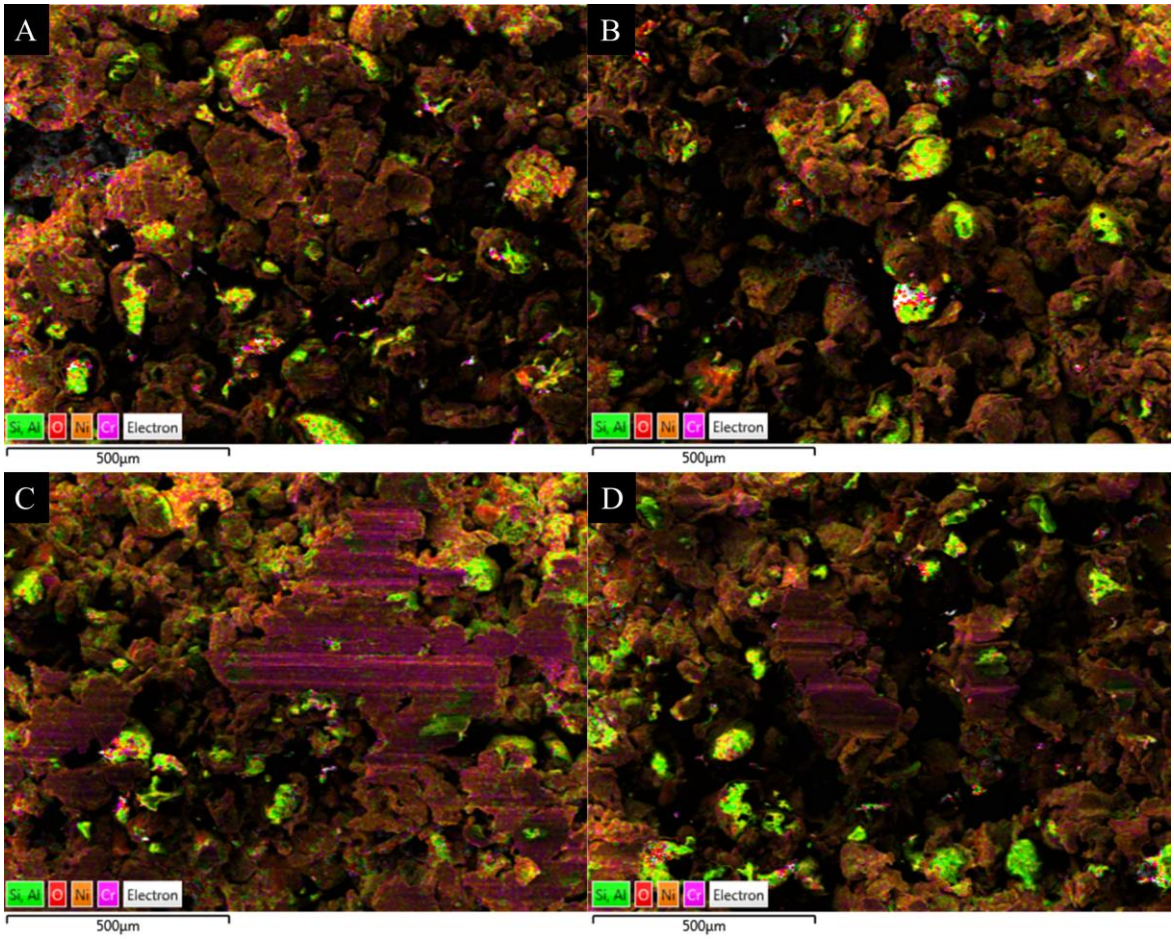

Figure 9 – a and b) EDS layered images for the abradable from repeat 1 in two locations c and d) EDS layered images for the abradable from repeat 2 in two locations.

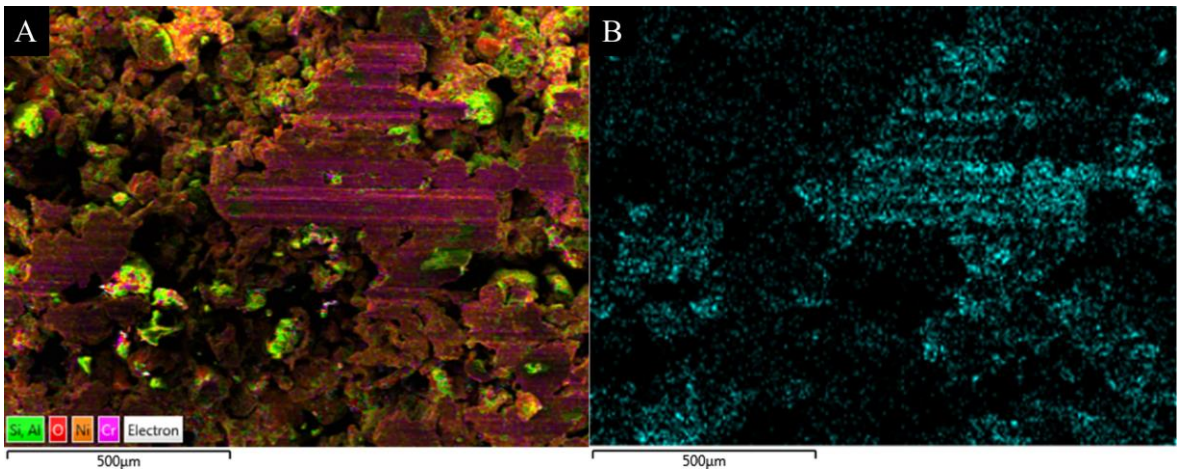

Figure 10 - a) EDS layered image for the abradable from repeat 2 in the first imaged location, b) Iron content EDS map in the same location.

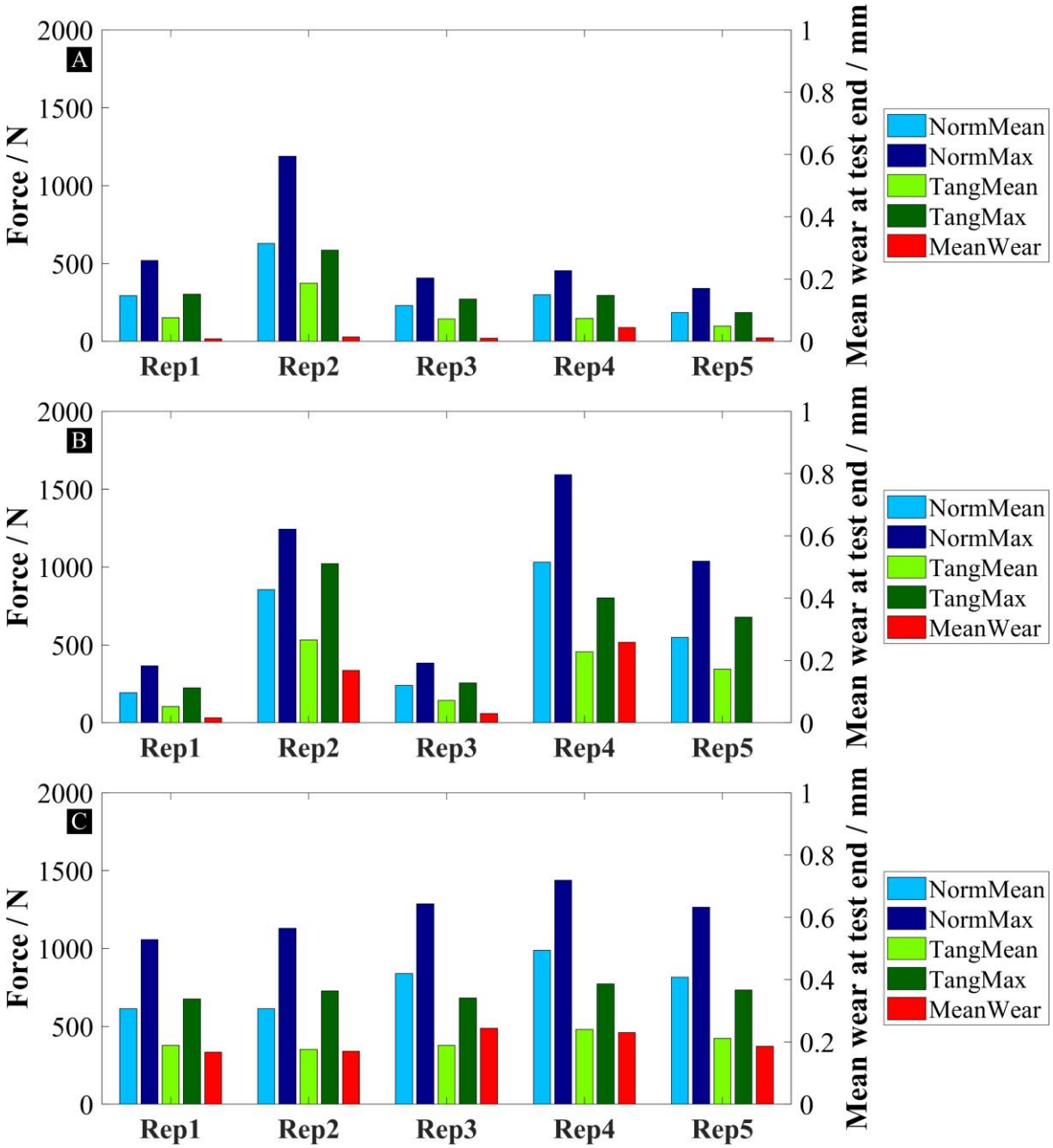

Figure 11 - The histograms showing the mean and maximum normal and tangential forces throughout a test and mean blade wear at the end of a test for each of the 5 repeats for tests at 200m/s speed and a) 0.06µm/pass incursion rate, b) 0.10µm/pass incursion rate, c) 0.14µm/pass incursion rate.

3.3 Transition incursion rate at 280m/s

For the results at the higher blade speed, once again, first a comparison of tests where transition was and was not observed is shown. This is then followed by a histogram summarising the test results for all 15 tests at 280m/s.

To illustrate the differences in wear behaviour between the tests that did not transition and that transitioned, a blade profile history map, accompanied by post-test images of the

abradable and blade and force data are shown for two tests. Figure 13 and Figure 14 show repeats 2 and 3 respectively at an incursion rate 0.22µm/pass, where repeat 2 transitioned to a high force wear mechanism.

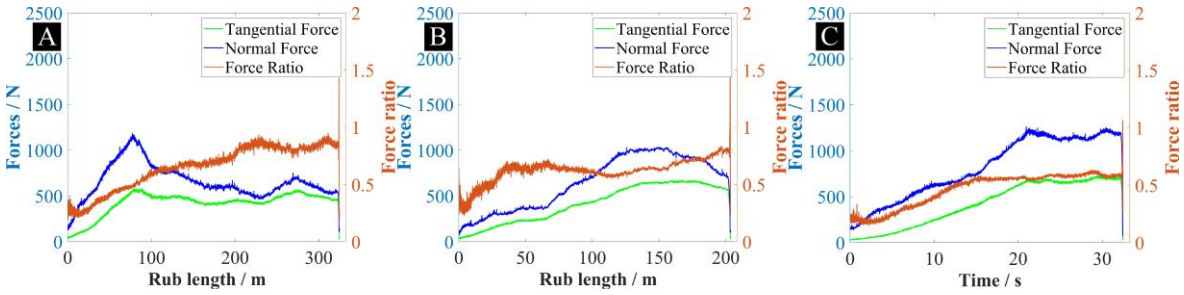

Figure 12 - Force results for the tests at 200m/s and a) repeat 2 at 0.06µm/pass, b) repeat 5 at 0.10µm/pass and c) repeat 5 at 0.14µm/pass.

In the case where transition did not occur, forces measured during the test were stable, with the normal force reaching approximately 450N (Figure 14b). Conversely, for the transitioned test (Figure 13b), the normal force reached approximately 1000N towards the end of the test, although it should be noted, the increase in force was not as rapid as for the transitioned test at 200m/s previously shown in Figure 7.

Considering the wear behaviour shown in the two Figures, the differences in wear between tests that transitioned and those that did not are similar to as observed at 200m/s. For the transitioned test, thermal damage can be seen on the blade in Figure 13c, and some shiny spots on the abradable surface in Figure 13e. Interestingly, on the blade history map in Figure 13a, it can also be seen that blade wear first started at the blade edges. This is likely related to blade temperature distribution, with the blade edge getting to hot temperatures first due to rubbing both the abradable under the blade and the sides of the blade. Figure 15 illustrates this with rubbing area shown in red, and localised increase in rubbing area for a unit width of a blade close to the sides shown with an arrow.

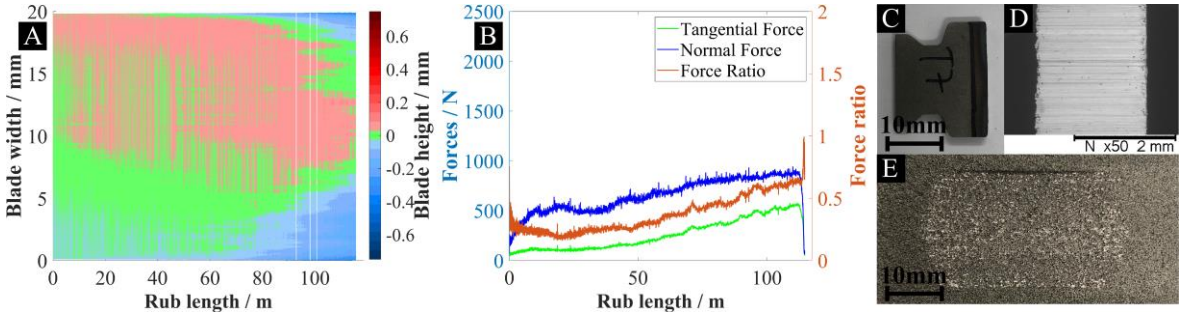

Figure 13 - Results for the repeat 2 at 0.22µm/pass, 200m/s with H50 abradable a) the blade profile history map, b) forces during the test, c) post-test image of the blade, d) post-test SEM of the blade, e) post-test image of the abradable sample. This test transitioned to the high-force contact mode.

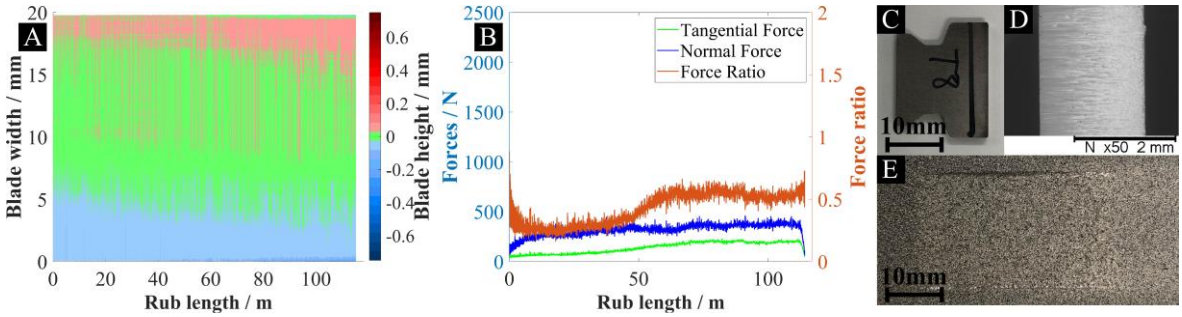

Figure 14 - Results for the repeat 3 at 0.22µm/pass, 200m/s with H50 abradable a) the blade profile history map, b) forces during the test, c) post-test image of the blade, d) post-test SEM of the blade, e) post-test image of the abradable sample. This test did not transition to the high-force contact mode.

The force and blade length results for all the 15 tests at 280m/s are summarised in Figure 16, where tests that transitioned to a high force wear mechanism are evident. As previously noted, the trend was similar to the tests at 200m/s. In this case, no tests had high forces at 0.14µm/pass, two tests at 0.22µm/pass and five tests at 0.30µm/pass. These results further support the view that the transition between the two contact modes occurs over a range of incursion rates for the samples in a given batch.

Once again, the two contact modes were distinct. As with the tests at 200m/s, higher blade wear was seen for the tests that transitioned to high forces. However, the ratio between the maximum force for the tests that transitioned and those that did not, was lower than for the tests at 200m/s. For example, for the tests at 0.22µm/pass and 280m/s, this ratio was around 2, while for the tests at 0.10µm/pass and 200m/s it was from 3 to 4.

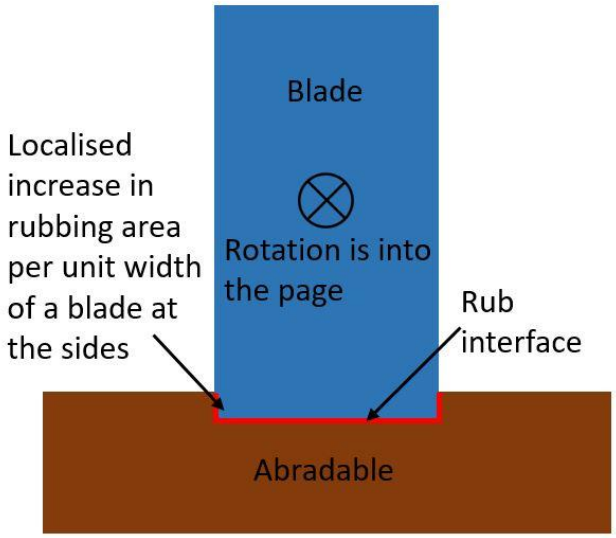

Figure 15 - A diagram showing the rubbing area between the blade edge and abradable and how localised increase in rubbing area per unit width of a blade occurs at the blade sides. Blade rotation direction is into the page.

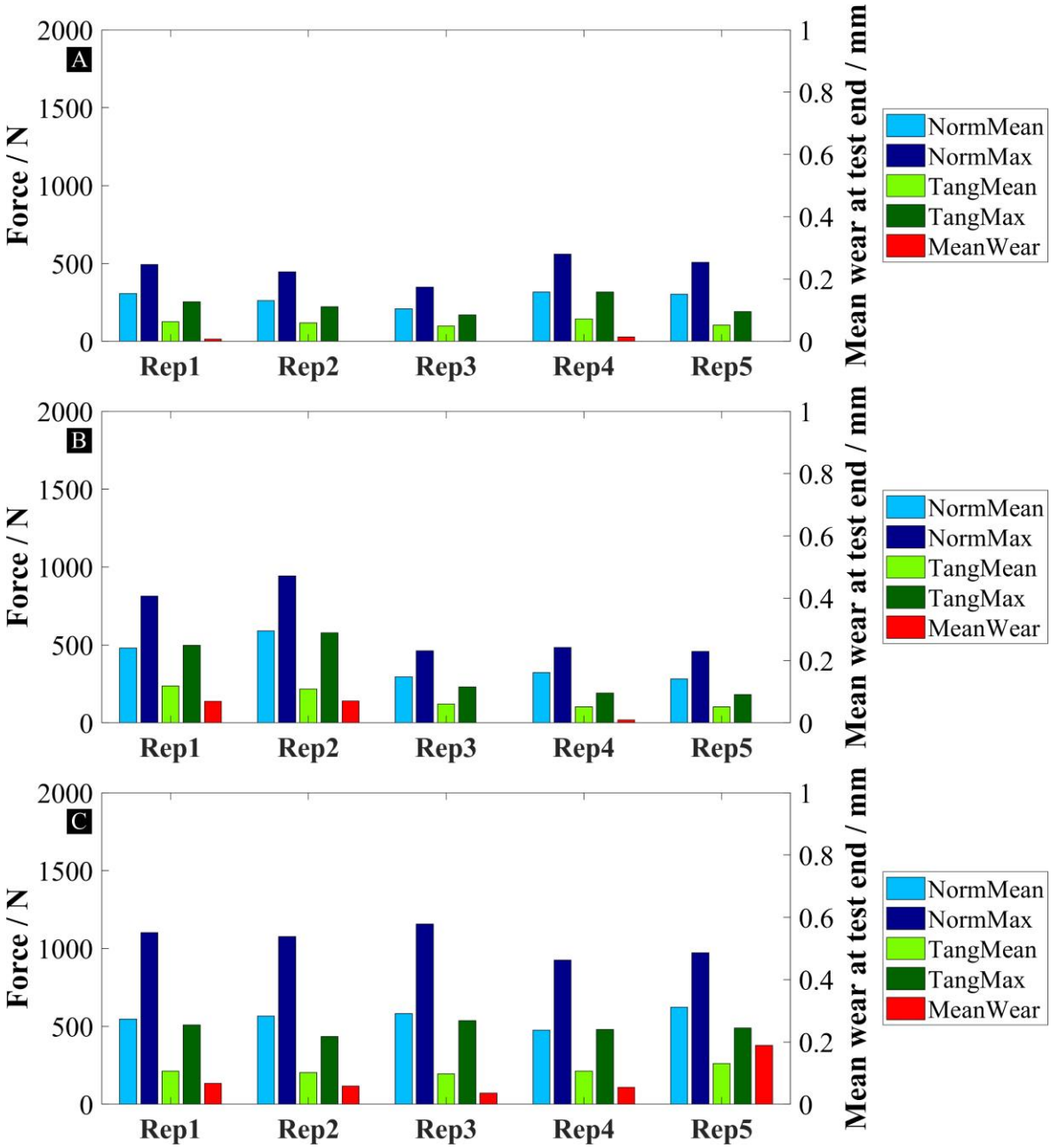

Figure 16 - The histograms showing the mean and maximum normal and tangential forces throughout a test and mean blade wear at the end of a test for each of the 5 repeats for tests at 280m/s speed and a) 0.14µm/pass incursion rate, b) 0.22µm/pass incursion rate, c) 0.30µm/pass incursion rate.

4 DISCUSSION

The results in this work can be used to further understand blade contacts with a NiCrAl-bentonite abradable, building on the findings of Taylor et al. [16] and Watson et al. [17, 18]. The abradable removal mechanism for all of the tests performed in this study was identified to be sub-surface damage accumulation and fracture. This was inferred from the rough as-sprayed like appearance of the abradable wear track, both for the tests that transitioned and

those that did not. This view was further supported by the SEM images of blades from the tests (Figure 6d, Figure 7d Figure 13d, and Figure 14d), as discolouration occurred on the trailing edge of all of the blades rather than on the tip of the leading edge, indicating that the work in fracturing the abradable is done by the whole blade thickness rather than just the tip, which is consistent with the suggested mechanism. The incursion rate and blade tip speed were similarly identified to be important in determining test outcomes, which is consistent with findings by Taylor et al. [16] and Watson et al. [17] where these two parameters as well as abradable hardness were identified to be important.

In addition to the above-mentioned parameters, the influence of rig stiffness and blade stick-out length (blade stiffness) on test outcomes were considered in this study. The rig stiffness was shown to not have a significant influence on test outcomes, as tests on both rigs produced similar results, with one out of three tests transitioning to the high-force contact mode for each of the rigs. This is despite the low-speed rig having a significantly less stiff arrangement than the high-speed rig (the low-speed rig having a cantilever arrangement and the high speed rig disc being supported by two sets of bearings – behind and in front of the disc). However, this result is perhaps not unexpected, due to the high contact speed (200-280m/s) and short arc of contact, resulting in a very short contact duration. This when combined with the relatively large disc radius (i.e. a large distance from the contact point to the disc support) leads to such stiffness differences being isolated from the contact between an abradable and a passing blade.

Similarly, a blade length difference between 4mm and 7mm was shown to not have a significant influence on the test outcomes. However, unlike the differences in rig stiffness, the differences in blade stiffness are local to the contact, meaning a different reason must account for their non-impact on the contact mechanic. Considering the blade / abradable system, both the 4mm and 7mm blades are significantly stiffer than the abradable itself (which has a significant amount of porosity in its structure). As such, whilst a change from 4mm to 7mm in terms of the length is significant in the context of the blade, it is less so relative to the overall system. In turn, both blades will have a similar influence on the energy transfer in the contact. Returning to Watson [17], energy transfer was identified as an important factor in determining abradable fracture effectiveness, and as such it is unsurprising the same material removal mechanic results for both blade lengths.

Additionally, it is also important to keep in mind that the range explored considering the influence of the blade length was small, with the primary aim being to gain an understanding of whether a change from a 7mm to a 4mm leads to significant changes in test outcomes. As such, further research is required into the stiffness of components local to the contact, such as that of a blade and an abradable to better understand how changes in stiffness of contacting components affect contact mechanisms, where it may well be that if blade length is extended considerably the wear mechanic does change.

4.1 The transition between the two contact modes

The results in this study provided new insights into the differences between blade/liner interactions with high and low contact forces, and into the transition between them. It was shown that even for identical test conditions, either contact mode might occur with the probability of the high force contact mode increasing with an increase in incursion rate. It was then suggested that the transition between two contact modes occurs not at a single incursion rate but over a range of incursion rates. The following can therefore be inferred:

- If the incursion rate is low, only the low-force contact mode would occur.
- In the transition region either mode could occur with a higher incursion rate increasing the likelihood of the high-force contact mode.
- If the incursion rate is high, only the high-force contact mode would occur.

The fact the transition occurs over a range of incursion rates is likely to be due to variations in sample hardness for samples within a given batch, with this highlighted in Section 2.1. These variations are due to the inherent randomness of the abradable spraying process [4], and are of particular significance given abradable hardness was previously shown to have a strong influence on the test outcomes [17]. This means that no two samples are identical and whilst a nominal transition incursion rate exists, it varies from sample to sample due to sample surface hardness variations.

Interestingly, it was observed that the differences between the two contact modes were very distinct, with the maximum normal force being two to four times (depending on the blade tip speed) larger for the tests in which the high-force contact mode occurred, in comparison to the tests in which the low-force contact mode occurred, for a given test condition. Such a sharp increase in the maximum normal force can be explained through the interactions between the incursion rate and the rate of abradable fracture. The low-force contact mode occurs when the rate of NiCrAl-bentonite fracture is the same as the incursion rate, so the forces remain stable. In turn, the forces stay low enough for Inconel 718 blades to not overheat and no significant blade wear occurs.

Conversely, the high-force contact mode occurs when NiCrAl-bentonite fractures slower than the incursion rate, leading to the build-up of force with time due to an effective increase in incursion rate per pass, as material from the previous incursion passes is not yet removed. The increase in force then continues until either forces are sufficient to continuously fracture the abradable for a given incursion rate, or until temperatures get high enough to initiate blade wear. Once blade wear initiates, it decreases the incursion rate experienced by an abradable sample, as part of the incursion rate is accommodated by blade wear, meaning equilibrium in terms of material removal and incursion rate is once again achieved. Finally, the presence of blade wear during the high-force contact mode is consistent with the results by Watson et al. [17], where it was shown that high forces were correlated with high temperatures and blade wear.

4.2 NiCrAl-bentonite abradable contact modes

The understanding gained in this study of the transition between the low-force and high-force contact modes, together with the findings from the identified previous studies, allows for a more complete overview of the contact between Inconel 718 blades and NiCrAl-bentonite abradables to be formed. In particular, this study has focused on the low-force and high-force contact modes. For the case of the low-force contact mode, abradable fracture was able to keep up with the incursion rate and contact forces remained stable for the whole duration of a test with no blade wear occurring. For the case of the high-force contact mode the abradable fracture was not fast enough to accommodate the incursion rate and forces kept increasing until part of the incursion rate was accommodated through blade wear, resulting in another steady force state with a much larger normal contact force than for the case of the low-force contact mode.

Based on the literature [16, 17], a third contact mode, which was not considered in this study exists at very high incursion rates (in the order of 2µm/pass for a NiCrAl-bentonite abradable with a similar nominal hardness to that used in this study) where significant abradable compaction occurred. Such a contact mode could be explained through the framework used to describe the low-force and high-force contact modes in the preceding section, in so much as at a very high incursion rate NiCrAl-bentonite fractures much slower than the incursion rate and forces increase rapidly. In particular, the test duration time at such a high incursion rate is likely to be insufficient for the blade to undergo significant thermal wear, and accommodate the remainder of the incursion. The forces then rise to a level sufficient to cause a significant macro-scale compaction in the abradable, with this consistent with the mechanism suggested for abradable compaction in the study by Watson et al. [17]. The compaction then leads to a very large increase in abradable surface hardness, contact forces and then potentially the subsequent rupture of the abradable. It is also notable that where Watson showed blade deformation at high incursion rates, that this was not accompanied by thermal damage, with this observation in support of the aforementioned comments on heating time being required for wear.

The three contact modes observed in the contacts between Inconel 718 blades and NiCrAl-bentonite abradables and their impact on test outcomes are summarised in Table 3.

Table 3 – Summary of the contact modes in the contacts between Inconel 718 blades and NiCrAl-bentonite abradables

Contact mode	Incursion rate accommodation mechanism	Contact force	Blade wear	Abradable macro-scale compaction
Low-force	Abradable fracture	Low	Low	Not significant

High-force	Abradable fracture+blade wear	High	Medium to high depending on the amount of incursion rate that is accommodated by blade wear	Not significant
Abradable compaction	Abradable fracture+blade wear+abradable compaction	Very high	Medium to high but not sufficient to accommodate enough of the incursion rate	Significant

Considering the boundaries in the table, the incursion rate at which progression from the low-force contact mode to the high-force contact mode occurs and then the likely transition from the high-force contact mode to the abradable compaction contact mode depends on a number of factors.

Previous research has identified that the incursion rate and abradable hardness are the dominant factors in contacts between NiCrAl-bentonite abradables and Inconel 718 blades, with the blade tip speed also playing an important role [16, 17]. This study has further supported the previously observed influences of the incursion rate and blade tip speed, and goes some way to explaining the reasons behind their significance. Indeed, based on the work in this study, the influences of these parameters can be linked to their effects on the effectiveness of abradable surface fracture due to damage accumulation. The effect of hardness can be explained by higher hardness decreasing the amount of abradable fracture due to the higher density of the NiCrAl phase. Similarly, the incursion rate influences the number of blade strikes an abradable surface experiences for a given rub depth, whilst also increasing the force of each strike as the material overlap increases. This suggests that not only the contact force is important in fracturing NiCrAl-bentonite surface, but also the total number of blade strikes (lower incursion rate leads to the higher number of blade strikes for a given incursion depth) with fatigue of the surface layer being important for effective surface removal. Finally, the increase in the blade tip speed likely improves the transfer of kinetic energy to the abradable surface increasing the amount of damage per blade strike as was suggested by Watson et al [17]. Both the effects of incursion rate and blade tip speed represent topics that could be explored through further work, and ultimately result in a unified model for material removal from a NiCrAl-bentonite abradable system, where an incursion rate, blade speed and hardness can be used to determine the wear mechanism likely to occur.

5 CONCLUSIONS

The results in this study allowed new insights into contacts between the Inconel 718 blades and NiCrAl-bentonite abradables that occur at a number of stages in the hot end of the compressor, in aero-engines that utilise abradable linings as clearance control systems.

The transition between the low-force and high-force contact modes was studied in detail and it was shown that the transition between the two contact modes occurs not at a single incursion rate but over a range of incursion rates. In addition, the results in this study offered further support to the sub-surface damage accumulation and fracture mechanism hypothesised by Watson et al. [17].

The contact modes were then explained through the balance between the incursion rate and the rates of abradable fracture, blade wear and abradable compaction. It is important to note, however, that the explanation is based primarily on the secondary observations such as contact forces and blade length changes during a test, and post-test analysis of blade and abradable samples. Direct experimental measurements of interactions between incursion rate and the rate of abradable fracture and blade wear would be useful to provide further evidence and can be an area for future research.

6 BIBLIOGRAPHY

[1] Z. Wang, A. Kulkarni, S. Deshpande, T. Nakamura and H. Herman, "Effects of pores and interfaces on effective properties of plasma sprayed zirconia coatings," *Acta Materialia,* vol. 51, p. 5319–5334, October 2003. https://doi.org/10.1016/S1359-6454(03)00390-2.

[2] H. I. Faraoun, J. L. Seichepine, C. Coddet, H. Aourag, J. Zwick, N. Hopkins, D. Sporer and M. Hertter, "Modelling route for abradable coatings," *Surface and Coatings Technology,* vol. 200, p. 6578–6582, June 2006. https://doi.org/10.1016/j.surfcoat.2005.11.105.

[3] B. Berthoul, A. Batailly, M. Legrand, L. Stainier and P. Cartraud, "Abradable Coating Removal in Turbomachines: A Macroscopic Approach Accounting for Several Wear Mechanisms," in *Volume 7B: Structures and Dynamics*, 2015. https://doi.org/10.1115/gt2015-42500.

[4] S. Wilson, "Thermally sprayed abradable coating technology for sealing in gas turbines," in *The Future of Gas Turbine Technology, 6th International Conference*, 2012.

[5] M. Yi, J. He, B. Huang and H. Zhou, "Friction and wear behaviour and abradability of abradable seal coating," *Wear,* vol. 231, p. 47–53, June 1999. https://doi.org/10.1016/s0043-1648(99)00093-9.

[6] X. Ma and A. Matthews, "Investigation of abradable seal coating performance using scratch testing," *Surface and Coatings Technology,* vol. 202, p. 1214–1220, December 2007. https://doi.org/10.1016/j.surfcoat.2007.07.076.

[7] X. Ma and A. Matthews, "Evaluation of abradable seal coating mechanical properties," *Wear,* vol. 267, p. 1501–1510, September 2009. https://doi.org/10.1016/j.wear.2009.03.044.

[8] M. O. Borel, A. R. Nicoll, H. W. Schlapfer and R. K. Schmid, "The wear mechanisms occurring in abradable seals of gas turbines," *Surface and Coatings Technology,* Vols. 39-40, p. 117–126, December 1989. https://doi.org/10.1016/0257-8972(89)90046-7.

[9] M. Bounazef, S. Guessasma and B. A. Saadi, "The wear, deterioration and transformation phenomena of abradable coating BN–SiAl–bounding organic element, caused by the friction between the blades and the turbine casing," *Materials Letters,* vol. 58, p. 3375–3380, November 2004. https://doi.org/10.1016/j.matlet.2004.02.049.

[10] J. Stringer and M. B. Marshall, “High speed wear testing of an abradable coating,” *Wear,* Vols. 294-295, p. 257–263, July 2012. https://doi.org/10.1016/j.wear.2012.07.009.

[11] N. Fois, M. Watson and M. B. Marshall, “The influence of material properties on the wear of abradable materials,” *Proceedings of the Institution of Mechanical Engineers, Part J: Journal of Engineering Tribology,* vol. 231, p. 240–253, August 2016. https://doi.org/10.1177/1350650116649528.

[12] N. Fois, “Investigation And Characterisation Of The Wear Mechanics Of Abradable Compressor Linings,” Ph.D dissertation, The University of Sheffield, 2015. [Online]. Available: https://etheses.whiterose.ac.uk/10723/

[13] N. Zhang, J. Shen, H. Xuan, Y. Hu and W. Hong, “Evaluation of an AlSi-polyester abradable seal coating performance using high-temperature and high-velocity abrasion tests,” *Proceedings of the Institution of Mechanical Engineers, Part J: Journal of Engineering Tribology,* vol. 230, p. 842–851, December 2015. https://doi.org/10.1177/1350650115619150.

[14] W. H. Xue, S. Y. Gao, D. L. Duan, Y. Liu and S. Li, “Material transfer behaviour between a Ti6Al4V blade and an aluminium hexagonal boron nitride abradable coating during high-speed rubbing,” *Wear,* Vols. 322-323, p. 76–90, January 2015. https://doi.org/10.1016/j.wear.2014.10.001.

[15] W. Xue, S. Gao, D. Duan, J. Zhang, Y. Liu and S. Li, “Effects of blade material characteristics on the high-speed rubbing behavior between Al-hBN abradable seal coatings and blades,” *Wear,* Vols. 410-411, p. 25–33, September 2018. https://doi.org/10.1016/j.wear.2018.06.003.

[16] T. A. Taylor, B. W. Thompson and W. Aton, “High speed rub wear mechanism in IN-718 vs. NiCrAl–Bentonite,” *Surface and Coatings Technology,* vol. 202, p. 698–703, December 2007. https://doi.org/10.1016/j.surfcoat.2007.05.054.

[17] M. Watson and M. Marshall, “Wear mechanisms at the blade tip seal interface,” *Wear,* Vols. 404-405, p. 176–193, June 2018. https://doi.org/10.1016/j.wear.2018.03.009.

[18] M. Watson, “Modifications of blade tips in abradable contacts,” Ph.D dissertation, The University of Sheffield, 2017. [Online]. Available: https://etheses.whiterose.ac.uk/18396/

[19] E. Rahimov, M. Watson, A. Hadjisoteriou and M. Marshall, “Investigation of wear mechanisms in AlSi-polyester abradable - Ti(6Al4V) blade contacts using stroboscopic imaging,” *Wear,* Vols. 494-495, p. 204207, April 2022. https://doi.org/10.1016/j.wear.2021.204207.

[20] N. Fois, J. Stringer and M. B. Marshall, “Adhesive transfer in aero-engine abradable linings contact,” *Wear,* vol. 304, p. 202–210, July 2013. https://doi.org/10.1016/j.wear.2013.04.033.

[21] H. Wang, “Criteria for analysis of abradable coatings,” *Surface and Coatings Technology,* vol. 79, p. 71–75, February 1996. https://doi.org/10.1016/0257-8972(95)02443-3.

[22] A. F. Emery, J. Wolak, S. Etemad and S. R. Choi, “An experimental investigation of temperatures due to rubbing at the blade-seal interface in an aircraft compressor,” vol. 91, no. 2, 1983. https://doi.org/10.1016/0043-1648(83)90248-X.

[23] S. Metals, “Inconel Alloy 718, Publication Number SMC-045,” 2007. [Online]. Available: https://www.specialmetals.com/documents/technical-bulletins/inconel/inconel-alloy-718.pdf. [Accessed 21 April 2024].